

One-pot synthesis and characterization of a mixture of Ga₂O₃ and SnO₂ nanofibers

Je-Myung Jeong^a, Yong Jung Kwon^b, Hong Yeon Cho^b, Han Gil Na^b and Hyoun Woo Kim^{b,*}

^aDepartment of Electronic Engineering, Hanyang University, Seoul 133-791, Korea

^bDepartment of Materials Science and Engineering, Hanyang University, Seoul 133-791, Korea

We have achieved simultaneous production of gallium oxide (Ga₂O₃) and tin oxide (SnO₂) one-dimensional (1D) nanostructures by heating a mixture of GaN and Sn powders at 900°C. X-ray diffraction and transmission electron microscopy analysis revealed that the product corresponded to a mixture of monoclinic Ga₂O₃ nanofibers and tetragonal rutile SnO₂ nanofibers. We suggest the growth mechanisms of Ga₂O₃ nanofibers and SnO₂ nanofibers to be vapor-solid and vapor-liquid-solid processes, respectively. The photoluminescence (PL) measurement with a Gaussian fitting exhibited visible light emission bands in the blue, yellow-green, and orange regions. The PL spectrum of the mixture of Ga₂O₃ and SnO₂ nanofibers was a combination of the PL spectra from the Ga₂O₃ and SnO₂ nanostructures.

Key words: Ga₂O₃, SnO₂, Nanostructures.

Introduction

Nanostructures are attracting great attention due to their novel physical properties [1-20]. Among these, one-dimensional (1D) nanostructures show potential applications to nanoelectronics and optoelectronics [21-27]. Several researchers have studied on the growth of Ga₂O₃ 1D nanostructures by various techniques [28-30] since gallium oxide (Ga₂O₃) is a stable wide-bandgap compound with intense luminescence properties [23]. In addition, tin oxide (SnO₂), an n-type semiconductor with a wide band gap ($E_g = 3.6$ eV at 300 K), is regarded as one of the most promising materials for gas sensors, heat mirrors, photovoltaic solar energy conversion devices, and transparent electrodes [31-33]. Accordingly, various structural and morphological forms of SnO₂ 1D nanostructures have been fabricated over the past several years [34-36].

With the development of nanoscience and nanotechnology, many researchers are interested in tailoring or improving the characteristics of nanostructures by synthesizing a wide variety of nanowires as well as developing a novel fabrication method. Although the 1D nanostructures of Ga₂O₃ and SnO₂ have previously been synthesized by the thermal heating of GaN and Sn powders, respectively, to the best of our knowledge, attempts to fabricate a mixture of both products have not been made.

Since both Ga₂O₃ and SnO₂ nanowires are useful materials, the mixture of the two materials is likely to

create extraordinary applications. For example, a mixture of Ga₂O₃ and SnO₂ nanowires would result in a chemical sensor with exceptionally high selectivity.

In this paper, we explore the use of a mixture of GaN and Sn powders for producing 1D nanostructures. We investigate the structural and photoluminescence (PL) properties, as well as the morphology and composition of the product. This study paves the way to prepare and characterize a mixture of nanostructures with various types of materials, which enables us to tailor or modify various useful properties.

Experimental

The synthesis was carried out in a quartz tube mounted vertically inside a high-temperature tube furnace. A mixture of GaN and Sn powders was placed on the alumina holder in the center of the quartz tube. For preparing the gold (Au)-coated Si substrates, we used Si as the starting materials (p-type (100) Si; resistivity = 1-30 Ω cm), onto which a layer of Au (about 3 nm) was deposited by a sputtering process. The furnace was heated to 900 °C, and maintained at this temperature for 2 h in a flow of nitrogen (N₂) gas (flow rate; 500 standard cm³/min). The tube was then cooled down naturally to room temperature in about 8 h.

As-grown samples were investigated and analyzed using glancing angle (0.5 °) X-ray diffraction (XRD, X'pert MPD-Philips with CuKα₁ radiation), scanning electron microscopy (SEM, Hitachi S-4200), and transmission electron microscopy (TEM, Philips CM-200) with energy-dispersive X-ray spectroscopy (EDX) attached. The PL spectra of the samples were measured in a SPEC-1403 photoluminescence spectrometer with a He-Cd laser (325 nm, 55 mW) at room temperature.

*Corresponding author:
Tel : +82-2-2220-0382
Fax: +82-2-2220-0389
E-mail: hyounwoo@hanyang.ac.kr

Results and Discussion

We found a large piece of wool-like products on the surface of the substrate. Fig. 1(a) shows a low-magnification SEM image, indicating that the product consists of a large quantity of straight or curved 1D structures. Statistical observation of many SEM images indicated that the average diameter of the 1D structures ranged from 10 to 500 nm. Fig. 1(b) shows the typical XRD pattern of the product. The reflection peaks of $(11\bar{1})$, (202) , (113) , $(11\bar{5})$, (300) , (213) , $(31\bar{3})$, (220) , and (222) correspond to a monoclinic Ga_2O_3 structure with lattice constants of $a = 5.80 \text{ \AA}$, $b = 3.04 \text{ \AA}$, and $c = 12.23 \text{ \AA}$ (JCPDS: 74-1176), whereas the diffraction peaks of (110) , (200) , (111) , (211) , (220) , (310) , (301) , and (321) can be readily indexed to the tetragonal rutile structure of SnO_2 with the lattice constants $a = 4.74 \text{ \AA}$ and $c = 3.19 \text{ \AA}$ (JCPDS: 41-1445). No obvious reflection peaks from impurities, such as unreacted Sn, Ga or other oxides, were detected. In the present XRD measurements, the angle of the incident X-ray beam to the surface of substrate was about 0.5° , with the detector being rotated to scan the samples. Since the peaks mainly originated from the products, the XRD analysis indicated that the well-crystallized Ga_2O_3 and SnO_2 were successfully obtained through the present synthetic route.

Fig. 2 is a low magnification TEM image, indicating that there are two types of 1D structure in the product: those without tip-nanoparticles (indicated by Arrow 1) and those with tip-nanoparticles (indicated by Arrow 2).

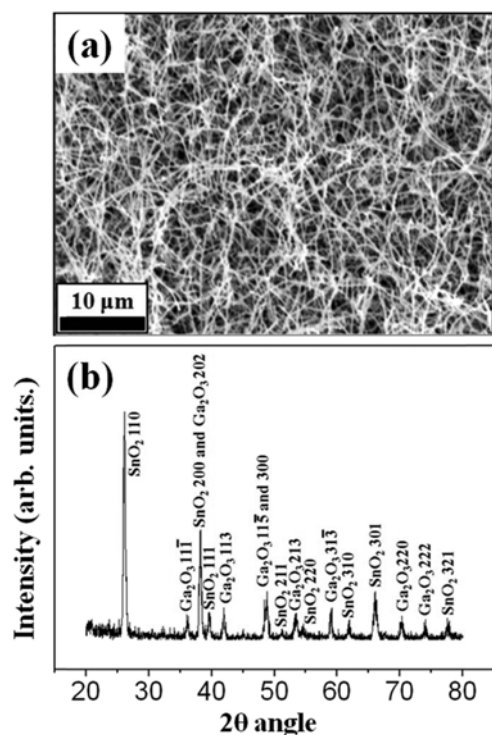


Fig. 1. (a) Low-magnification SEM image of the product. (b) XRD patterns recorded from the product.

Fig. 3(a) shows a TEM image of a single nanofiber indicated by Arrow 1 in Fig. 2, in which the nanofiber has a diameter of about 62 nm. The upper right inset in Fig. 3(a) shows the associated selected area electron diffraction (SAED) pattern. The SAED pattern can be indexed for the $[1\bar{1}0]$ zone axis of crystalline Ga_2O_3 .

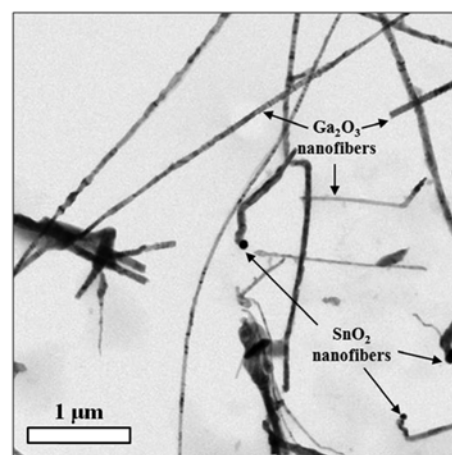


Fig. 2. Low-magnification TEM image of the product. SnO_2 nanofibers exhibit the tip nanoparticles, whereas Ga_2O_3 nanofibers do not.

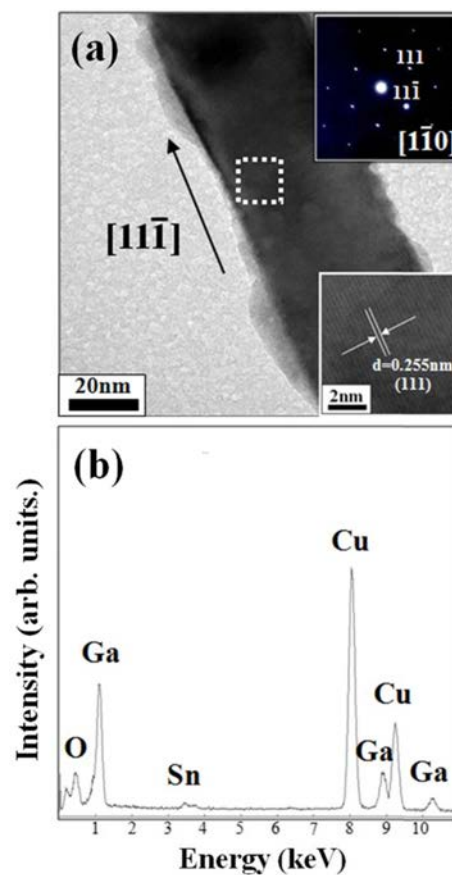


Fig. 3. (a) TEM image of a single nanofiber indicated by Arrow 1 in Fig. 2 (Upper right inset: associated SAED pattern; lower right inset: HRTEM image enlarging an area enclosed by the square in Fig. 3(a)). (b) EDX spectrum collected from the nanofiber shown in Fig. 3(a).

The length direction of the nanofiber is along the $[1\bar{1}\bar{1}]$ direction. The lower right inset is a high resolution TEM (HRTEM) image enlarging an area enclosed by the square in Fig. 3(a), revealing good crystallinity. The interplanar spacing is about 0.255 nm, corresponding to the (111) plane of monoclinic Ga_2O_3 . Fig. 3(b) shows the typical EDX spectrum collected from the nanofiber shown in Fig. 3(a). The spectrum identifies the peaks of Ga, O, Sn, and Cu. Since the Cu signals are generated from the TEM microgrid supporting the nanofibers, we suppose that the components of the nanofiber are Ga, O, and a trace amount of Sn. From the XRD, SAED, and HRTEM observation, in which the nanofiber is monoclinic Ga_2O_3 , we suggest that Sn exists in an element in the Ga_2O_3 lattice.

Fig. 4(a) shows the TEM image of a single nanofiber indicated by Arrow 2 in Fig. 2 (average diameter ~ 83 nm). The nanoparticle at the tip of the nanofiber appears dark, having high contrast compared with the nanofiber stem. The inset in Fig. 4(a) shows the corresponding SAED pattern, which can be indexed for the $[10\bar{2}]$ zone axis of the tetragonal rutile SnO_2 . Fig. 4(b) is the enlarged HRTEM image of the rectangular box marked in Fig. 4(a). The interplanar spacing is approximately 0.176 nm, corresponding to the (211) plane of the tetragonal rutile SnO_2 . EDX measurements made on the fiber tip and the fiber stem indicate that the tip consists of Au, Sn, O, and Ga (Fig. 4(c)), but the stem is only composed of Sn, O, and Ga (Fig. 4(d)). Accordingly, we reveal that the SnO_2 nanofibers contain a trace amount of Ga, while the nanoparticle comprises a Au element.

In the preliminary experiments, the synthesis was carried out under the same conditions as those in the present work, with the exception that only Sn powders

were used. In this case, 1D nanostructures of SnO_2 without tip nanoparticles were obtained. When only GaN powders were used, Ga_2O_3 1D nanostructures without tip nanoparticles were obtained. In the present work, however, although the Ga_2O_3 nanofibers still do not have nanoparticles at their tips, the SnO_2 nanofibers revealed the presence of tip nanoparticles. In other words, it is noteworthy that the growth mechanism was changed with the change in the source composition. SnO_2 nanofibers with tip nanoparticles were not obtained when only the Sn precursors as the source were used, whereas those with tip nanoparticles were produced by using a mixture of GaN and Sn powders.

We suppose that the mixing of the source powders will affect the growth mechanism. In general, there are two main growth mechanisms of 1D nanostructures: vapor-liquid-solid (VLS) and vapor-solid (VS) mechanisms. It is expected that the growth mode is dependent on the experimental condition. In the VLS mode, the generated vapor combines with Au on the substrate and the supersaturation of the liquid alloy droplet brings about the precipitation of short nuclei from which the nanowires may subsequently grow [37]. On the other hand, in the VS mode, the catalytic role of Au will be reduced, and the nanowires will tend to grow by direct adsorption of the source vapors onto the solid substrate [38].

In a previous study, the growth temperature determines the relevant growth mode, in which lower and higher temperature growth were dominated by the VLS and VS processes, respectively [38]. Higher temperature guarantees higher vapor pressure of the source materials. Similarly, at the growth temperature in the present work, sufficient amount of source vapor is provided. Furthermore, we expect that the relative amount of Ga concentration is significantly greater than that of the Sn concentration in the vapor of the present system. Accordingly, most Ga vapors will directly adsorb on the substrate and nanowire surface, being operated by the VS process. On the other hand, the relatively small amount of Sn vapors at that temperature will bring about a situation, in which the ratio of the Sn-associated vapor to Au is expected to be sufficiently small.

The existence of Au-related tip nanoparticles suggests that the growth of SnO_2 nanofibers is mainly controlled by a VLS process, with Au originating from the pre-deposited Au layer. In the present synthetic process, liquid Sn (Melting point = 232°C) is oxidized, according to the reaction of $2\text{Sn(l)} + \text{O}_2(\text{g}) \rightarrow 2\text{SnO(g)}$. We believe that the oxygen comes from the air leakage or the residual oxygen in the furnace, even though we did not intentionally introduced oxygen to the tube. The generated metastable SnO gas spontaneously decomposes into liquid Sn and solid SnO_2 ($2\text{SnO(g)} \rightarrow \text{SnO}_2(\text{s}) + \text{Sn(l)}$) [39-42]. The liquid Sn droplets fall on the substrate and subsequently form Sn-Au alloyed

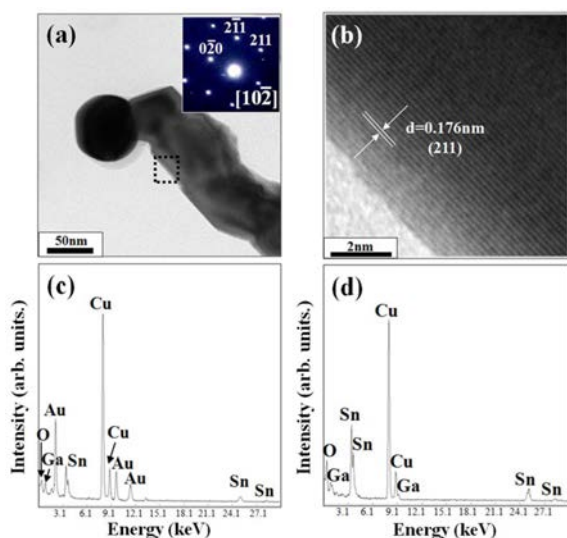


Fig. 4. (a) TEM image of a single nanofiber indicated by Arrow 2 in Fig. 2 (Inset: corresponding SAED pattern). (b) Enlarged HRTEM image of a rectangular box marked in Fig. 4(a). EDX spectra of (c) the fiber tip and (d) the fiber stem.

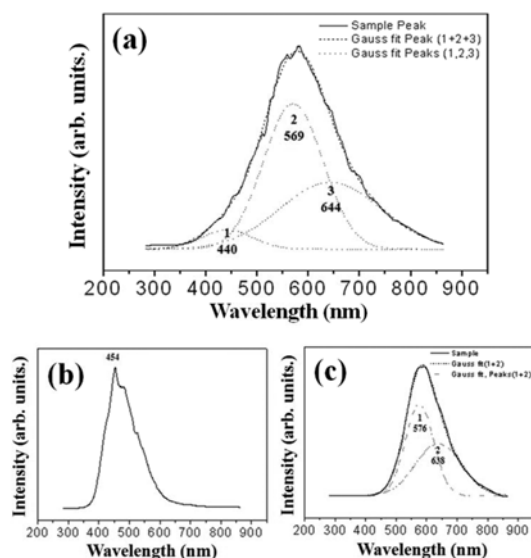


Fig. 5. (a) PL spectrum of the product synthesized by heating a mixture of GaN and Sn powders. The solid line is the experimental spectrum and the dotted lines are the Gaussian deconvolution. The PL spectra of the products obtained by heating (b) the pure GaN and (c) the pure Sn powders.

droplets, which provide energetically favored sites for adsorption of the SnO and O vapor [43]. Subsequently, as the concentrations of the Sn and O atoms in the alloy droplets or nanoparticles become greater than the saturation threshold, the short SnO₂ nuclei precipitate from the solid/liquid interface. In the next step, by continuously dissolving SnO and O onto the nanoparticles, solid SnO₂ nanofibers may subsequently grow.

On the other hand, the GaN powders are evaporated into Ga and N gases when they are heated at 900 °C, according to the reaction: $4\text{GaN(s)} \rightarrow 4\text{Ga(g)} + 2\text{N}_2\text{(g)}$ [44]. A large amount of Ga vapor directly deposits on the substrate or on the surface of the fibers and reacts with the O atoms. Accordingly, the VS mechanism dominates the growth process of the Ga₂O₃ nanofibers. This is evidenced by the observation that no catalyst was present at the tips of Ga₂O₃ nanofibers (Fig. 2). It is noteworthy that only Ga₂O₃ or SnO₂ was found in the product, without the formation of a Ga_xSn_yO_z compound phase. This observation agrees with previous work reporting that the GaO_{1.5}-SnO₂ binary consists entirely of a two-phase region between the two endpoints [45], with minimal solubility of GaO_{1.5} into SnO₂ or SnO₂ into GaO_{1.5} [46]. The intermediate compound, Ga₄SnO₈, which has been reported to be stable at temperatures higher than ~1300 °C [46, 47], does not form in the present synthetic process at 900 °C.

The PL spectrum at room temperature is shown in Fig. 5(a). If using Gaussian fitting, we can find that the PL spectrum consists mainly of three bands, peaking at about 440 (2.83 eV), 569 (2.18 eV), and 644 nm (1.93 eV), in the blue, yellow-green, and orange region, respectively. For comparison, we measured the PL

spectra of the Ga₂O₃ 1D nanostructures (Fig. 5(b)) and the SnO₂ 1D nanostructures (Fig. 5(c)). The 1D nanostructures of Ga₂O₃ and SnO₂ were produced when pure GaN powders and pure Sn powders were heated at 900 °C, respectively. The blue emission band, which is shown in Figs. 5(a) and 5(b), is known to be attributed to Ga vacancies (V_{Ga}), O vacancies (V_{O}) [48], and a Ga-O vacancy pair ($V_{\text{Ga}}, V_{\text{O}}$) in Ga₂O₃ [49]. The products also show an emission band in the yellow-green region (Figs. 5(a) and 5(c)), being similar to that of the SnO₂ 1D nanostructures previously synthesized by using laser ablation [50] and solution phase growth [51]. In addition, we observed an orange band as shown in Fig. 5(a) and 5(c). Similarly, orange emission has been previously observed from sintered SnO₂ [52]. The visible light emission of SnO₂ is known to be related to defects, such as O vacancies or Sn interstitials that form during the synthesis process [50-53]. In consideration of a possible measurement error during the Gaussian fitting analysis, we suggest that the PL spectrum of the mixture of Ga₂O₃ and SnO₂ nanofibers is a combination of the PL spectra from the Ga₂O₃ and SnO₂ nanostructures, respectively. Further detailed study is in progress in order to reveal the emission mechanism in detail.

Conclusions

In summary, we simultaneously fabricated crystalline Ga₂O₃ and SnO₂ nanofibers by heating a mixture of GaN and Sn powders at 900 °C. We used XRD, SEM, TEM, and EDX spectroscopy to characterize the samples. The product consists of 1D nanostructures with diameters in the range of 10 to 500 nm. The Ga₂O₃ nanofibers have a monoclinic structure, whereas the SnO₂ nanofibers have a tetragonal rutile structure. The Ga₂O₃ and SnO₂ nanofibers contain a trace amount of Sn and Ga elements, respectively. Based on the observation of the nanofiber tips, we suggest that the growth of the Ga₂O₃ and SnO₂ nanofibers is mainly controlled by the VS and VLS mechanisms, respectively. The relatively large amount of Ga vapors contributes to the growth of the Ga₂O₃ nanofibers via the VS mechanism. On the other hand, the small ratio of Sn to Au atoms in the system activates the Au catalytic effect, which is operated by the VLS mechanism. The PL measurement with a Gaussian fitting shows apparent visible light emission bands centered at 440, 569, and 644 nm, indicating that the blue emission can be attributed to the Ga₂O₃ nanofibers, whereas the yellow-green and the orange emissions are ascribed to the SnO₂ nanofibers.

Acknowledgments

This research was supported by the Basic Science Research Program through the National Research

Foundation of Korea (NRF) funded by the Ministry of Education, Science and Technology (2011-0009946).

References

- R. Kuar, M. C. Mishra, B. K. Sharma, V. Vyas and G. Sharma, *Electron. Mater. Lett.* 9 (2013) 19-23.
- H.-W. Cui, D.-S. Li and Q. Fan, *Electron. Mater. Lett.* 9 (2013) 1-5.
- M. A. Majeed Khan, W. Khan, M. Ahamed, M. S. Alsalthi and T. Ahmed, *Electron. Mater. Lett.* 9 (2013) 53-57.
- R. Sabbaghizadeh and M. Hashim, *Electron. Mater. Lett.* 9 (2013) 115-118.
- D. Soundararajan, Y. Lim, M.-P. Chen and K. H. Kim, *Electron. Mater. Lett.* 9 (2013) 177-182.
- T. Prakash, S. Ramasamy and B. S. Murty, *Electron. Mater. Lett.* 9 (2013) 207-211.
- A. Mondal, J. C. Dhar, P. Chinnamuthu, N. K. Singh, K. K. Chatopadhyay, S. K. Das, S. Ch Das and A. Bhattachayya, *Electron. Mater. Lett.* 9 (2013) 213-217.
- S. N. Heo, K. Y. Park, Y. J. Seo, F. Ahmed, M. S. Anwar and B. H. Koo, *Electron. Mater. Lett.* 9 (2013) 261-265.
- S. Sharma and S. Chawla, *Electron. Mater. Lett.* 9 (2013) 267-271.
- K. Seo, M. Suh and S. Ju, *Electron. Mater. Lett.* 9 (2013) 273-277.
- C.-H. Lee, D.-J. Choi and Y.-J. Oh, *Electron. Mater. Lett.* 9 (2013) 283-286.
- Y. Jia, F. Yang, F. Cai, C. Cheng and Y. Zhao, *Electron. Mater. Lett.* 9 (2013) 287-291.
- S. Kim, G. Nam, K. G. Yim, J. Lee, Y. Kim and J.-Y. Leem, *Electron. Mater. Lett.* 9 (2013) 293-298.
- H.-W. Cui, D.-S. Li and Q. Fan, *Electron. Mater. Lett.* 9 (2013) 299-307.
- H. Lee, J.-H. Shin, J. Chae, J. B. Kim, T.-H. Kim and K.-B. Park, *Electron. Mater. Lett.* 9 (2013) 357-362.
- S. Kumar, P. Dharma and V. Sharma, *Electron. Mater. Lett.* 9 (2013) 371-374.
- T. Sreesattabud, B. J. Gibbons, A. Watcharapasom and S. Jiansirisomboon, *Electron. Mater. Lett.* 9 (2013) 409-412.
- N.-M. Park, J. Shin, B. Kim, K. H. Kim and W.-S. Cheong, *Electron. Mater. Lett.* 9 (2013) 467-469.
- C.-G. Kuo, H. Chang, L.-R. Hwang, S. Hor, J.-S. Chen, G.-Y. Liu and S.-C. Cheng, *Electron. Mater. Lett.* 9 (2013) 481-484.
- J. Huang, S. Somu and A. Busnaina, *Electron. Mater. Lett.* 9 (2013) 505-507.
- E. W. Wong, P. E. Sheehan and C. M. Lieber, *Science* 277 (1997) 1971-1975.
- J. T. Hu, T. W. Odom and C. M. Lieber, *Acc. Chem. Res.* 32 (1999) 435-445.
- Z. W. Pan, Z. R. Dai and Z. L. Wang, *Science* 291 (2001) 1947-1949.
- L. F. Dong, J. Jiao, D. W. Tuggle, J. Petty, S. A. Elliff and M. Coulter, *Appl. Phys. Lett.* 82 (2003) 1096-1098.
- H. W. Seo, C.-S. Han, W. S. Jang and J. Park, *Curr. Appl. Phys.* 6 (2006) e216-e218.
- S. J. Jo, D. K. Lee, M.-S. Kim, Y. H. Kim and Y. S. Kang, *Curr. Appl. Phys.* 6 (2006) 781-785.
- H. Hasegawa, *Curr. Appl. Phys.* 7 (2007) 318-321.
- Y. C. Choi, W. S. Kim, Y. S. Park, S. M. Lee, D. J. Bae, Y. H. Lee, G. S. Park, W. B. Choi, N. S. Lee and J. M. Kim, *Adv. Mater.* 12 (2000) 746-750.
- C. H. Liang, G. W. Meng, G. Z. Wang, Y. W. Wang, L. D. Zhang and S. Y. Zhang, *Appl. Phys. Lett.* 78 (2001) 3202-3204.
- G. Gundiah, A. Govindaraj and C. N. R. Rao, *Chem. Phys. Lett.* 351 (2002) 189-194.
- Z. M. Jarzebski and J. P. Maraton, *J. Electrochem. Soc.* 123 (1976) 199-205.
- Q. V. Vasu and A. Subrahmanyam, *Thin Solid Films* 193/194 (1990) 973-980.
- A. Tsunashima, *J. Mater. Sci.* 21 (1986) 2731-2734.
- R.-Q. Zhang, Y. Lifshitz and S.-T. Lee, *Adv. Mater.* 15 (2003) 635-640.
- Z. L. Wang and Z. Pan, *Adv. Mater.* 14 (2002) 1029-1032.
- Y. Liu, C. Zheng, W. Wang, C. Yin and G. Wang, *Adv. Mater.* 13 (2001) 1883-1887.
- H. W. Kim, M. A. Kebede, H. S. Kim, H. G. Na, J. C. Yang, C. Lee, *Met. Mater. Int.* 16 (2010) 87-91.
- S. S. Kim, J. Y. Park, H. S. Kim, H. G. Na, J. C. Yang, S. H. Shim, C. Lee, D. Park, D. Nam, H. Cheong, H. W. Kim, *J. Phys. D: Appl. Phys.* 44 (2011) b025502.
- J. Q. Hu, X. L. Ma, N. G. Shang, Z. Y. Xie, N. B. Wong, C. S. Lee and S. T. Lee, *J. Phys. Chem. B* 106 (2002) 3823-3826.
- D.-W. Yuan, R.-F. Yan and G. Simkovich, *J. Mater. Sci.* 34 (1999) 2911-2920.
- J. C. Nover and F. D. Richardson, *Trans. Inst. Min. Metall.* 81 (1972) 63.
- Z. R. Dai, Z. W. Pan and Z. L. Wang, *Adv. Funct. Mater.* 13 (2003) 9-24.
- J. X. Wang, D. F. Liu, X. Q. Yan, H. J. Yuan, L. J. Ci, Z. P. Zhou, Y. Gao, L. Song, L. F. Liu, W. Y. Zhou, G. Wang and S. S. Xie, *Solid State Commun.* 130 (2004) 89-94.
- J.-S. Lee, K. Park, S. Nahm, S.-W. Kim and S. Kim, *J. Cryst. Growth* 244 (2002) 287-295.
- G. B. Palmer and K. R. Poepfelmeier, *Solid State Sci.* 4 (2002) 317-322.
- D. D. Edwards and T. O. Mason, *J. Am. Ceram. Soc.* 81 (1998) 3285-3292.
- M. B. Varfolomeev, A. S. Miranova, T. I. Dudina and Koldashov, *Russ. J. Inorg. Chem.* 20 (1975) 1738.
- L. F. Dong, J. Jiao, M. Coulter and L. Love, *Chem. Phys. Lett.* 376 (2003) 653-658.
- N. Sakulchaicharoen and D. E. Resasco, *Chem. Phys. Lett.* 377 (2003) 377-383.
- J. Hu, Y. Bando, Q. Liu and D. Goldberg, *Adv. Funct. Mater.* 13, (2003) 493-496.
- B. Cheng, J. M. Russell, W. Shi, L. Zhang and E. T. Samulski, *J. Am. Chem. Soc.* 126 (2004) 5972-5973.
- D. Maestre, A. Cremades and J. Piqueras, *J. Appl. Phys.* 95 (2004) 3027-3030.
- S.-S. Chang and D. K. Park, *Mater. Sci. Eng. B* 95 (2002) 55-60.